Chinese Chemical Letters 34 (2023) 107883

Contents lists available at ScienceDirect

Chinese Chemical Letters

journal homepage: www.elsevier.com/locate/cclet

Self-assembly of porphyrins on perovskite film for blade-coating stable large-area methylammonium-free solar cells

Taorui Liu, Yajun Liu, Xingbang Gao, Jing Cao*

State Key Laboratory of Applied Organic Chemistry, Key Laboratory of Nonferrous Metal Chemistry and Resources Utilization of Gansu Province, College of Chemistry and Chemical Engineering, Lanzhou University, Lanzhou 730000, China

ARTICLE INFO

Article history:
Received 28 July 2022
Revised 5 September 2022
Accepted 4 October 2022
Available online 10 October 2022

Keywords:
MA-free perovskite
Ni porphyrin
Supramolecule
Self-assemble
Phase transition
Phase separation

ABSTRACT

Phase transition and phase separation of formamidinium-cesium (FA-Cs) perovskite during the fabrication and operation processes reduce the efficiency and stability of perovskite solar cells (PSCs). Here, we develop an *in situ* molecular self-assembly approach on perovskite surface using an amine nickel porphyrin (NiP). The NiP doped perovskite precursor solution was deposited on substrate by blade-coating under ambient condition. NiP molecules self-assemble into supramolecule bound on perovskite surface during the vacuum-assisted process. Such a modification controls the perovskite grain growth to generate the uniform perovskite film. The supramolecule can release the residual lattice strain to inhibit the phase transition of perovskite film, and promote the charge extraction and transport to suppress the phase separation of FA-Cs perovskite during long-term illumination condition. Consequently, the best efficiency of large-area NiP-based FA-Cs-PSCs with the active area of 1.0 cm^2 is up to 20.3% (certified as 19.2%), which is close to the record efficiency (20.37%) by blade-coating. Unencapsulated NiP-doped device reveals the remarkably improved overall stabilities. This work affords a novel way to address the phase transition and phase separation in FA-Cs perovskite.

Organic-inorganic hybrid perovskite solar cells (PSCs) have attached tremendous attention due to their excellent photovoltaic properties and low-cost solution processing techniques [1–4]. The power conversion efficiency (PCE) of PSCs has rapidly improved up to 25.7% [5–8]. Among the perovskite materials used in PSCs, methylammonium (MA)-perovskites reveal the poor stability at high temperature or under light illumination, which is negative to the commercial application of devices [9–11]. By comparison, formamidinium (FA)-based perovskite materials with suitable bandgap exhibit broader light absorption spectra extending to 840 nm, thereby yielding the great cell performance. Especially, they have the better thermal stability, rendering FA cation promising candidate for the organic cation in perovskite [12–14]. However, the photoactive $FAPbI_3$ is thermodynamically stable only above 150 °C, which rapidly changes to the yellow δ-phase at room temperature [15–18]. Effectively controlling the phase transition to avoid the generation of δ-phase is essential to optimize the PCE and stability of FA-based devices.

Some efforts have been made to understand the mechanism behind the phase transition of FA-based perovskites. For instance, Zhu and his coworkers found that the intrinsic instability of α-phase $FAPbI_3$ came from the anisotropic strained lattice in the (111) plane, which caused the transition from α to δ phase [19]. Researchers deeply investigated the cause of strained lattice and found that larger FA ions could distort the cage of PbI_6 octahedra and therefore generate the strain in perovskite lattice [20,21]. The yielded lattice strain was mainly concentrated at perovskite interface, thereby resulting in the degradation of perovskite film [22,23]. Several approaches had been developed to stabilize the α-phase $FAPbI_3$ at room temperature, including the construction of 2D/3D hybrid perovskite [24,25], surface functionalization engineering [26,27], and composition engineering [28–30], adding Cs ion into FA perovskite (FA-Cs) for the stabilization of perovskite lattice was considered as an applicable way to stabilize the α-phase $FAPbI_3$ perovskite films, especially for large-area devices [31,32]. However, the crystallization process of FA-Cs perovskite remains largely uncontrollable, then resulting in the poor quality perovskite films with large number of pinholes [33,34]. Additionally, the phase separation is easily generated in the FA-Cs perovskite film under long-term continuous illumination condition

* Corresponding author.
E-mail address: caoj@lzu.edu.cn (J. Cao).

https://doi.org/10.1016/j.cclet.2022.107883
1001-8417/

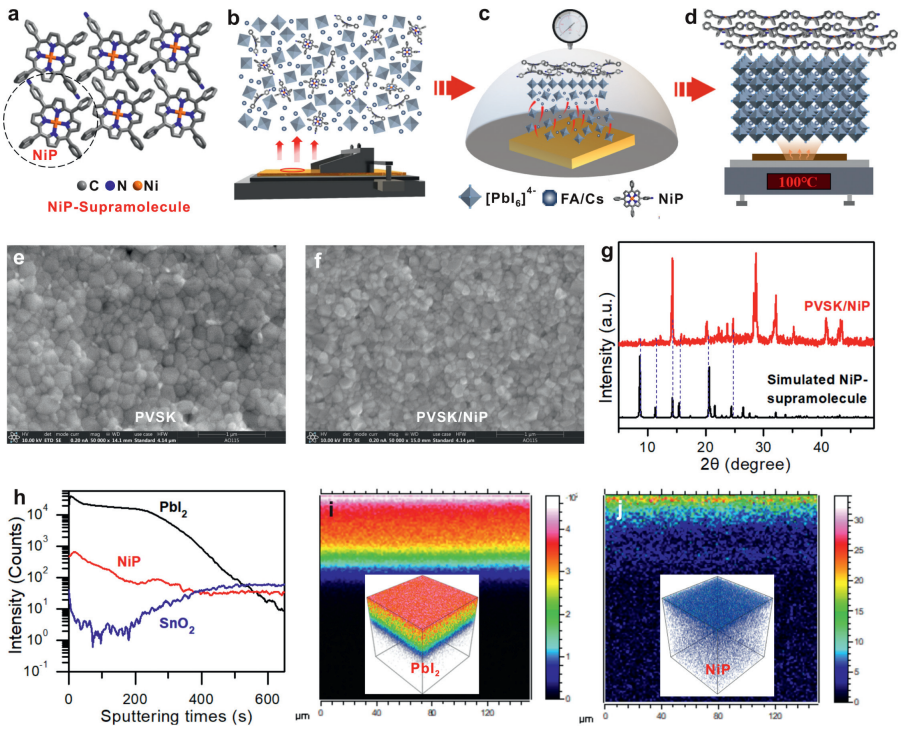

Fig. 1. (a) Structure of NiP-supramolecule. Fabricated process of perovskite (PVSK) film: (b) blade-coating in ambient environment (c) vacuum-assisted crystallization process (d) annealed at 100 °C to obtain dense film. Surface SEM images of PVSK films without (e) and with (f) NiP doping. (g) Powder XRD patterns of PVSK film with NiP doping and simulated value of NiP-supramolecule. (h) Fragments distribution in NiP-doped PVSK film. TOF-SIMS profiles of (i) PbI_2, (j) NiP components from the top to bottom in NiP-doped PVSK film.

[35,36]. These issues are detrimental to the performance and overall stability of FA-Cs-based PSCs. Thus, how to simultaneously address the phase transition and phase separation in FA-Cs perovskite film is still a challenge, which is rarely studied at current stage.

Porphyrins and their derivatives with good thermal stabilities and charge transport properties have been demonstrated as a promising surfactant in perovskite film [37,38]. Here, a surfactant-like monoamine nickel porphyrin (NiP) was directly doped into FA-Cs perovskite precursor solution to prepare perovskite film by blade-coating under ambient condition. During the vacuum-assisted crystallization process, the NiP molecules rapidly self-assembled into supramolecule (Fig. 1a) on the top surface of perovskite film to control the film growth and defects formation. The introduced NiP-supramolecules bound on perovskite film surface effectively released the residual lattice strain and further inhibited the phase transition of $FAPbI_3$ from α to δ phase. Approaching record efficiency as 20.31% (20.37% for the record performance prepared by blade-coating [39]) for blade-coating large-area (1.0 cm^2) FA-Cs-based PSCs with NiP-supramolecule was unprecedentedly realized in ambient environment, which was further certified as 19.16% with an area of 1.0014 cm^2. More importantly, the bound supramolecule layer boosted the efficient interfacial charge extraction and transport from perovskite layer, thus to suppress phase separation of FA-Cs perovskite. The unencapsulated PSCs with NiP-supramolecule exhibited the remarkably enhanced overall stabilities, such as the photostability by maintaining an initial efficiency of 80% under AM 1.5 G solar light continuous illumination over 1300 h.

In this work, the perovskite composition being $Cs_{0.05}FA_{0.95}PbI_3$ was employed as the light absorber to fabricate MA-free perovskite films. Surfactant-like NiP was doped in the precursor solution to prepare the FA-Cs perovskite films by vacuum-assisted blade-coating method (Figs. 1b-d, the detailed prepared process shown in Experimental Section). Scanning electron microscopy (SEM) images revealed that the introduction of NiP modulated the crystallization process of FA-Cs perovskite film and reduced the surficial pinholes, thus to yield a dense perovskite film with more homogeneous grain size (Figs. 1e and f, Figs. S1 and S2 in Supporting information). X-ray diffraction (XRD) pattern of NiP-doped perovskite powder was in good agreement with the simulated value obtained from the crystal structure of NiP-supramolecule (Fig. 1g), clearly verifying that the introduced NiP molecules was self-assembled into supramolecule within perovskite film. The consistent UV–visible spectra of perovskite films without and with NiP doping (Fig. S3 in Supporting information) indicated that the doped NiP-supramolecule did not enter the perovskite lattice and change the perovskite composition. Time flight secondary ion mass spectrometry (TOF-SIMS) tests were further conducted to assess the dispersed position of NiP-supramolecule in perovskite film. As shown in Figs. 1h-j, the NiP-supramolecule was mainly deposited on the surface of perovskite film, probably attributable to the rapid crystallization of NiP-supramolecule during vacuum-assisted process. We found by Infrared Radiation (IR) and X-ray photoelectron spectroscopy (XPS) test that the organic cations in perovskites could protonate NiP molecules in supramolecule to generate the ammonium porphyrins ($NiP\text{-}H^+$) (Figs. S4 and S5 in Supporting information) [38,40]. Figs. S6-S9 (Supporting information) further demonstrate they will be anchored on perovskite grain surface. Thus, we can conclude that with the assistance of vacuum process, the introduced NiP molecules in perovskite film self-assemble into supramolecule to *in situ* anchor on the surface of perovskite film. Such a modification adjusts the crystallization process of perovskite film and reduces the film defects generation, resulting in the fabrication of high-quality FA-Cs perovskite film.

The components of perovskite films without and with NiP-supramolecule were evaluated by the XRD measurements. As illustrated in Fig. 2a, the peak at 11.8° in the pristine FA-Cs perovskite film indicated the presence of δ-phase $FAPbI_3$. In compar-

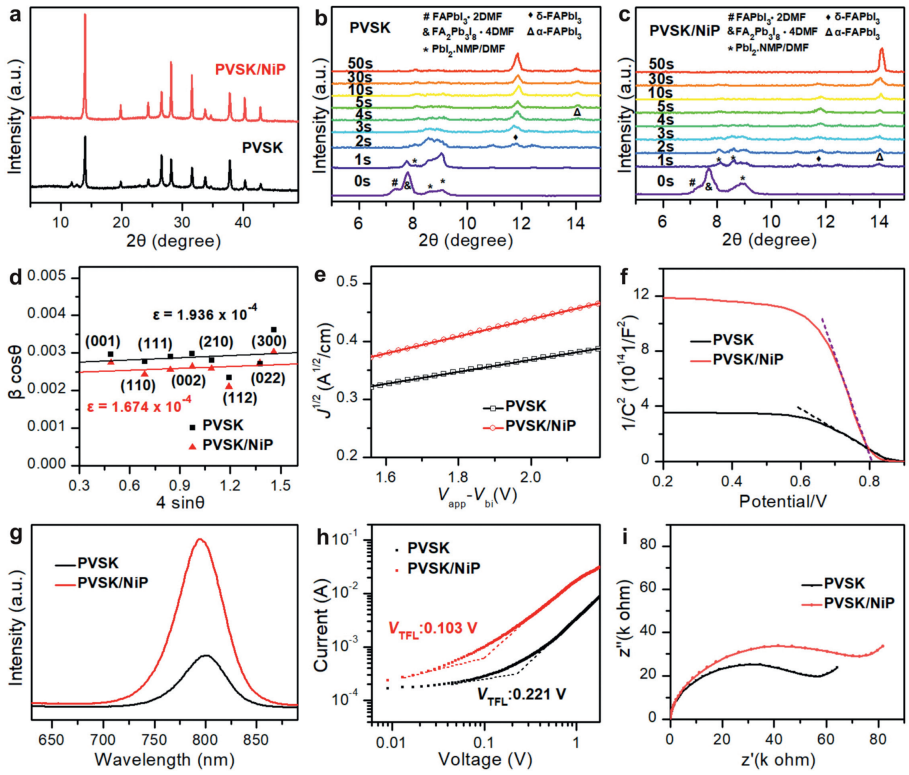

Fig. 2. (a) XRD patterns of PVSK films without and with NiP doping. XRD patterns of PVSK films (b) without and (c) with NiP doping during vacuum assist process. (d) Williamson-Hall plots of PVSK samples without and with NiP doping. (e) Hole mobilities, (f) Mott-Schottky analyses, (g) PL spectra, (h) Hole trap-state densities and (i) EIS plots of the devices without and with NiP doping.

ison, the film modified by NiP-supramolecule showed no obvious peak at 11.8°, which indicated the formation of δ-phase $FAPbI_3$ was effectively inhibited. To gain insights into the effect of NiP-supramolecule on the crystallization process of FA-Cs perovskite films, the UV–vis spectra of perovskite films with and without NiP doping were tested during vacuum-assisted process. As shown in Fig. S10 (Supporting information), compared to the pristine perovskite film, the NiP-doped perovskite film revealed a faster intensity increase around 400 nm and an earlier tendency to form perovskite phase [39]. The phase generation process of perovskite films was further investigated by XRD tests. As observed in Figs. 2b and c, the solvent-coordinated intermediate phase was formed in the films without and with NiP-supramolecule modification at the begging of vacuum-assisted process [7,33]. A significant δ-phase $FAPbI_3$ was yielded after 2 s vacuum treatment for the pristine perovskite film. By contrast, the α-phase $FAPbI_3$ was rapidly yielded in the NiP-doped perovskite film within 1 s after vacuum-assisted initiation. Additionally, the NiP-supramolecule modified film tended to form α-phase $FAPbI_3$ in the following vacuum treatment time. These findings verify that the supramolecule adjusts the growth of FA-Cs perovskite film, to preferentially generate a pure α-phase $FAPbI_3$ in the modified film.

Studies revealed that the lattice distortion induced by larger FA ions generated the lattice strain in FA-based perovskite film surface, further resulting in the spontaneous phase transition of $FAPbI_3$ film. The NiP-supramolecules modified on perovskite film would influence the lattice strain to maintain the α phase FA-Cs perovskite film at room temperature. To quantify the effect of supramolecule structure, we calculated the lattice strain in FA-Cs perovskite films by the simplified Williamson-Hall (WH) method (the detailed formula simplification procedure shown in Experimental Section in Supporting information) [41–43]:

$$\beta \cos\theta = \varepsilon(4 \sin\theta) \quad (1)$$

The magnitude of ε can be derived from the slope of $\beta\cos\theta$ *versus* $4\sin\theta$. We determined the values of β and θ from the XRD data (Fig. 2a) by Gaussian fit (Table S1 in Supporting information) to calculate the lattice strain in perovskite films. As prepared in Fig. 2d and Fig. S11 (Supporting information), the results revealed that the strain in supramolecule modified perovskite film (1.674×10^{-4}) was obviously reduced than that of pure perovskite film (1.936×10^{-4}), verifying that the NiP-supramolecules modified on perovskite film could release the lattice strain to inhibit the occurrence of phase transition in FA-based film.

Hole mobility tests were prepared to investigate the charge transportation ability of NiP-supramolecule modified FA-Cs perovskite film. As shown in Fig. 2e and Table S2 (Supporting information), the NiP-doped perovskite film has higher hole mobility with 2.99×10^{-4} cm^2 V^{-1} s^{-1} than that of pristine perovskite film with 1.48×10^{-4} cm^2 V^{-1} s^{-1}. In the Mott-Schottky test, the slope of the NiP-doped perovskite film was larger than the pristine perovskite film (Fig. 2f), exhibited lower interfacial charge density. These results verify the introduction of supramolecule facilitate the interfacial charge extraction and transport. Steady-state photoluminescence (PL) spectra revealed the modified perovskite film had a stronger FL intensity than the pristine perovskite film (Fig. 2g), suggesting that there had fewer defects in the modified film to suppress the non-radiative recombination. The densities of hole trap states of films without and with NiP doping were estimated to be 7.17×10^{15} cm^{-3} and 3.34×10^{15} cm^{-3} *via* the space-charge limited current (SCLC) measurement (Fig. 2h and Table S3 in Supporting information), further demonstrating that the NiP-supramoleule could passivate the interfacial defects to obtain high-quality α-phase $FAPbI_3$ film. In addition, the NiP-doped perovskite film exhibited a larger V_{oc} than the pristine perovskite film under light intensities. The ideality factor decreased from 1.18 for the pristine sample to 1.11 for the NiP-doped per-

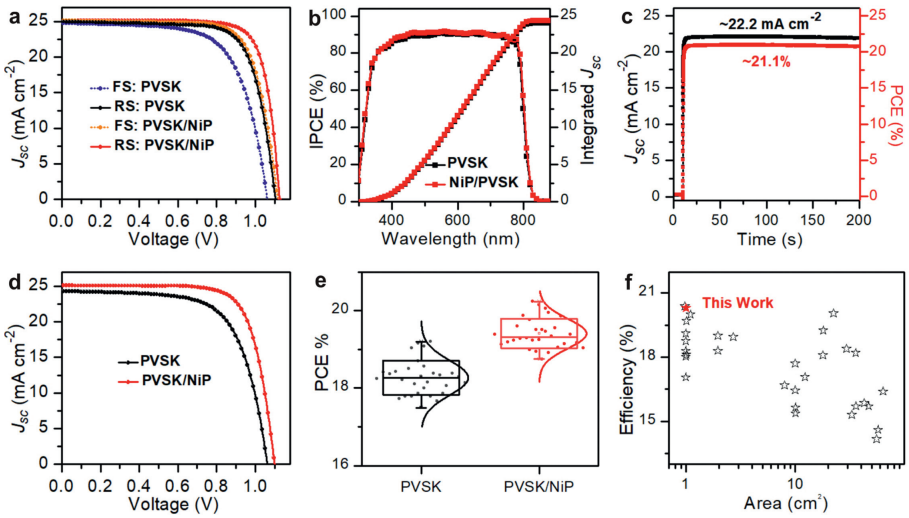

Fig. 3. (a) Best *J-V* data tested in reverse (RS) and forward (FS) scans of PSCs with an area of 0.1 cm^2. (b) IPCE of PSCs without and with NiP doping. (c) Stabilized power output of PCE and J_{sc} at maximum power point for the NiP-doped PSCs. (d) Best *J-V* data of large-area devices with 1.0 cm^2. (e) Statistical results of efficiencies among 30 large-area cells (1.0 cm^2). (f) Statistic of area *versus* efficiencies for blade-coating large-area PSCs from this work and recent representative reports.

ovskite film (Fig. S12 in Supporting information), which implied that the trap-assisted recombination is suppressed with the decrease of trap states by supramolecule modification. The larger recombination resistance for NiP-doped perovskite film was also observed than that of pure perovskite film by Nyquist plots of electrical impedance spectroscopy (EIS) (Fig. 2i). These results exhibit that NiP-supramolecules modified on the surface of perovskite film could reduce interfacial charge recombination and facilitates charge extraction and transport.

The PSC devices were fabricated with FTO/modified ZnO [44] /mesoporous TiO_2/perovskite/Spiro-OMeTAD structure to assess the function of NiP-supramolecule on the cell performance. As shown in Fig. 3a and Table S4 (Supporting information), the modification of NiP-supramolecule significantly reduce the hysteresis and improves the efficiency of the PSCs, and the best efficiency of the small area (0.1 cm^2) NiP-doped device is as high as 21.6%. The incident photon-to-current conversion efficiency (IPCE) spectra of the devices without and with NiP doping are in good agreement with their corresponding *J-V* test data (Fig. 3b). The stabilized efficiency output further evaluated NiP-doped device with the champion efficiency of 21.1% (Fig. 3c). Then, we blade-coated large-area perovskite films to verify the positive effect on the large-area PSCs by introducing supramolecule. As illustrated in Fig. 3d and Table S5 (Supporting information), the V_{oc} and FF were significantly increased with the modification of supramolecule. The average efficiency of large area PSCs with NiP doping was 19.4% ± 0.9%, while the control device was 18.2% ± 0.9% (Fig. 3e). Especially, the best efficiency of NiP-doped PSCs reached 20.31% for an area of 1.0 cm^2, which is close to the record efficiency (20.37% [39]) of large-area PSCs prepared by blade-coating (Fig. 3f and Table S5 in Supporting information). Eventually, the efficiency of PSCs with NiP doping was certified as 19.16% with an area of 1.0014 cm^2 (Fig. S13 in Supporting information). Therefore, the NiP-supramolecule modified on the perovskite surface promotes the charge extraction and transport to further improve the cell performance.

Since porphyrins have excellent hydrophobicity, NiP-doped perovskite film exhibit higher water contact angle compared to the pristine film (Fig. S14 in Supporting information). The stabilities of PSCs without and with NiP were tested with FTO/modified ZnO [44] /mesoporousTiO_2/perovskite/phth-alocyanine [45] without encapsulation. Moisture stability of PSCs was performed with the humidity of 65% at room temperature, the NiP-doped device maintained more than 80% of its initial efficiency after 800 h, while the control device was almost entirely disabled (Fig. 4a). Thermal stability of PSCs was carried out at 85 °C and ~55% humidity, as shown in Fig. 4b, the NiP-doped device retained over 80% of its initial efficiency after 1200 h, while the control PSC maintained only <40% of initial efficiency in the same time span. Photostability of the PSCs were tested at the AM 1.5 G illumination in N_2 atmosphere, the NiP-doped device maintained 80% of its original efficiency after 1300 h (Fig. 4c), whereas the control device failed rapidly after 450 h under the same condition.

The enhanced photostability of NiP-doped PSCs is of great significance to push the commercial application of FA-Cs-based PSCs. Researches pointed out that FA-Cs perovskite could generate Cs-rich clusters under long-term light exposure, resulting in photogenerated carrier transport hindrance. Such a situation led to the heterogeneous distributions of $CsPbI_3$ and $FAPbI_3$ phase to further generate phase separation [36,46]. This phenomenon severely impairs the performance of FA-based PSCs and limit their commercial application. To gain insights into the enhancement of the photostability in NiP-supramoleule modified FA-Cs PSCs, we subjected the perovskite films to AM 1.5 G illumination for 12 h aging. A shown in Figs. 4d and e, compared to the pristine perovskite film, the (001) crystalline peak of NiP-doped perovskite film in the XRD patterns was shifted with a smaller angle after 12 h illumination. Additionally, the pristine FA-Cs perovskite film generated a new peak at 9.5° assigned to the δ-phase $CsPbI_3$ after 12 h light exposure. We speculate from these results that the formation of the FA-rich phase was suppressed by NiP-supramoleule, which was further evaluated by the peak shift in PL emission. As shown in Fig. 4f, the aged NiP-doped perovskite film had a smaller red-shifted than the pristine perovskite film. These results indicate that the pristine perovskite film spontaneously generate FA-rich perovskite phase ($FA_{>0.95}Cs_{<0.05}PbI_3$) and Cs-rich perovskite phase ($FA_{<0.95}Cs_{>0.05}PbI_3$) after 12 h illumination [35,47]. In contrast, the phase separation was effectively suppressed in NiP-doped PSCs. Thus, we can conclude that NiP-supramolecules can release lattice strain and promote the charge extraction and transport, thereby to prevent the blocking and accumulation of photogenerated carrier. Thus, effectively suppressing the phase separation of FA-Cs perovskite and enhancing the photostability of PSCs.

In this work, we introduced NiP molecules into perovskite precursor solution to fabricate PSCs by vacuum-assisted blade-

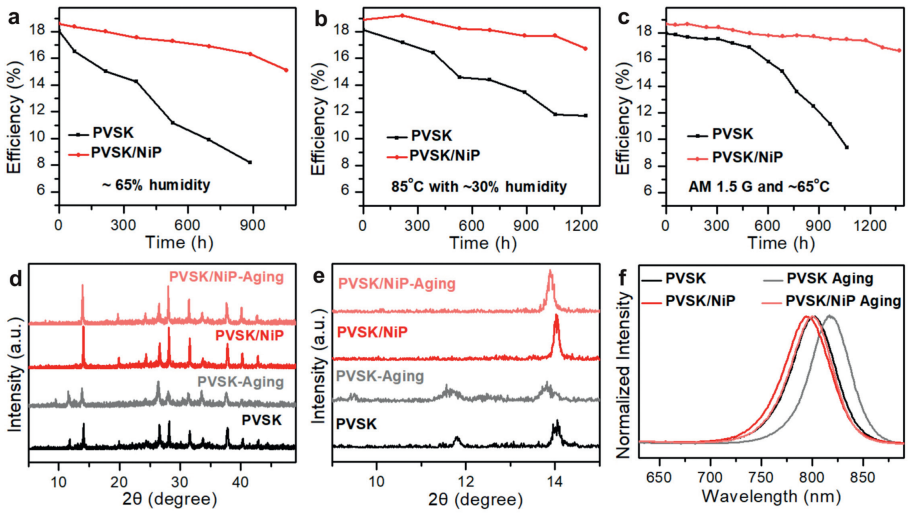

Fig. 4. Stability measurements at (a) ~65% humidity, (b) 85 °C with ~55% humidity, and (c) AM 1.5 G illumination and ~65 °C in N_2 atmosphere. The PVSK films were placed under AM 1.5 G illumination aged 0 h and 12 h. (d) XRD patterns, (e) enlarged XRD patterns from 9° to 15°, and (f) normalized PL spectra.

coating method. With the assistance of vacuum treatment, the NiP molecules self-assembled into NiP-supramolecule bound on perovskite film surface. The supramolecule adjusts the crystallization process of perovskite film to form high quality α-phase-dominated film and the lattice strain in FA-Cs perovskite film was released to inhibit the phase transition. Meanwhile, the formed NiP-supramolecule promoted hole extraction and transport to suppress the phase separation of perovskite film during continuous illumination. As a result, the large-area NiP-doped MA-free PSCs with PCE as high as 20.31% were fabricated with significantly enhanced photostability. Our work provides a promising approach for preparation of efficient and stable large-area FA-Cs-based PSCs.

Declaration of competing interest

The authors declare no competing financial interest.

Acknowledgments

We acknowledge the National Natural Science Foundation of China (No. 22075116), Fundamental Research Funds for the Central Universities of China (No. lzujbky-2021-ey10) and Science and Technology program of Gansu Province (No. 20JR5RA305).

Supplementary materials

Supplementary material associated with this article can be found, in the online version, at doi:10.1016/j.cclet.2022.107883.

References

[1] Y. Zhao, F. Ma, Z. Qu, et al., Science 377 (2022) 531–534.
[2] Z. Wei, Y. Zhao, J. Jiang, et al., Chin. Chem. Lett. 31 (2020) 3055–3064.
[3] M. Worku, A. Ben-Akacha, T. Blessed Shonde, et al., Small Sci. 1 (2021) 2000072.
[4] Y. Sun, W. Chen, Z. Sun, Chin. Chem. Lett. 33 (2022) 1772–1778.
[5] Y. Fang, L. Zhang, Y. Yu, et al., CCS Chem. 3 (2020) 2203–2210.
[6] Best Research-Cell Efficiency Chart; https://www.nrel.gov/pv/cell-efficiency.html
[7] T. Bu, L.K. Ono, J. Li, et al., Nat. Energy 7 (2022) 528–536.
[8] X. Jiang, K. Wang, H. Wang, et al., Small Sci. 1 (2021) 2000054.
[9] S.H. Turren-Cruz, A. Hagfeldt, M. Saliba, Science 362 (2018) 449–453.
[10] W.Q. Wu, P.N. Rudd, Q. Wang, Z. Yang, J. Huang, Adv. Mater. 32 (2020) e2000995.
[11] C. Ge, Z. Yang, X. Liu, et al., CCS Chem. 3 (2020) 2035–2044.
[12] J. Jeong, M. Kim, J. Seo, et al., Nature 592 (2021) 381–385.
[13] X. Ling, H. Zhu, W. Xu, et al., Angew. Chem. Int. Ed. 60 (2021) 27299–27306.
[14] R. Li, C. Li, M. Liu, et al., CCS Chem. 4 (2021) 3084–3094.
[15] H. Lu, Y. Liu, P. Ahlawat, et al., Science 370 (2020) eabb8985.
[16] Q. Jia, T. Shao, L. Tong, et al., Chin. Chem. Lett. 34 (2023) 107539.
[17] T. Du, T.J. Macdonald, R.X. Yang, et al., Adv. Mater. 34 (2022) e21078.
[18] C. Su, Z. Zhang, J. Yao, et al., Chin. Chem. Lett. 34 (2023) 107442.
[19] X. Zheng, C. Wu, S.K. Jha, et al., ACS Energy Lett. 1 (2016) 1014–1020.
[20] G. Kim, H. Min, K.S. Lee, et al., Science 370 (2020) 108–112.
[21] W. Hui, L. Chao, H. Lu, et al., Science 371 (2021) 1359–1364.
[22] J. Wu, Y. Cui, B. Yu, et al., Adv. Funct. Mater. 29 (2019) 1905336.
[23] Y. Chen, Y. Lei, Y. Li, et al., Nature 577 (2020) 209–215.
[24] J. Zhou, L. Ding, F. Zhao, et al., Chin. Chem. Lett. 31 (2020) 554–558.
[25] Z. Duan, G. Na, S. Wang, et al., Small Sci. 2 (2022) 2100114.
[26] F. Wang, W. Geng, Y. Zhou, et al., Adv. Mater. 28 (2016) 9986–9992.
[27] G.B. Xiao, Z.F. Yu, J. Cao, Y. Tang, CCS Chem. 2 (2020) 488–494.
[28] N.J. Jeon, J.H. Noh, W.S. Yang, et al., Nature 517 (2015) 476–480.
[29] S. Tang, Y. Deng, X. Zheng, et al., Adv. Energy Mater. 7 (2017) 1700302.
[30] G.B. Xiao, L.Y. Wang, X.J. Mu, et al., CCS Chem. 3 (2021) 25–36.
[31] Z. Yang, W. Zhang, S. Wu, et al., Sci. Adv. 7 (2021) eabg3749.
[32] R. Chen, Y. Wang, S. Nie, et al., J. Am. Chem. Soc. 143 (2021) 10624–10632.
[33] T. Bu, J. Li, H. Li, et al., Science 372 (2021) 1327–1332.
[34] L. Chao, T. Niu, W. Gao, et al., Adv. Mater. 33 (2021) e2005410.
[35] N. Li, Y. Luo, Z. Chen, et al., Joule 4 (2020) 1743–1758.
[36] Y. Deng, S. Xu, S. Chen, et al., Nat. Energy 6 (2021) 633–641.
[37] C. Li, J. Yin, R. Chen, et al., J. Am. Chem. Soc. 141 (2019) 6345–6351.
[38] Z. Fang, L. Wang, X. Mu, et al., J. Am. Chem. Soc. 143 (2021) 18989–18996.
[39] Q. Liang, K. Liu, M. Sun, et al., Adv. Mater. 34 (2022) e2200276.
[40] J.H. Zhao, X. Mu, L. Wang, et al., Angew. Chem. Int. Ed. 61 (2022) e202116308.
[41] J.T.W. Wang, Z. Wang, S. Pathak, et al., Energy Environ. Sci. 9 (2016) 2892–2901.
[42] G. Kim, H. Min, S.Lee Kyoung, et al., Science 370 (2020) 108–112.
[43] M. Ghasemi Hajiabadi, M. Zamanian, D. Souri, Ceram. Int. 45 (2019) 14084–14089.
[44] J. Cao, B. Wu, R. Chen, et al., Adv. Mater. 30 (2018) 1705596.
[45] Z. Yu, L. Wang, X. Mu, et al., Angew. Chem. Int. Ed. 60 (2021) 6294–6299.
[46] K. Ma, H.R. Atapattu, Q. Zhao, et al., Adv. Mater. 33 (2021) e2100791.
[47] Y. Zhou, F. Wang, Y. Cao, et al., Adv. Energy Mater. 7 (2017) 1701048.